Accessing Photoredox Transformations with an Iron(III) Photosensitizer and Green Light

Akin Aydogan,[1] Rachel E. Bangle,[2] Alejandro Cadranel,[3,4,5] Michael D. Turlington,[2] Daniel T. Conroy,[2] Emilie Cauët,[6] Michael L. Singleton,[1] Gerald J. Meyer,[2,*] Renato N. Sampaio,[7,*] Benjamin Elias[1,*] and Ludovic Troian-Gautier[1,2,8,*]

[1]Université catholique de Louvain (UCLouvain), Institut de la Matière Condensée et des Nanosciences (IMCN), Molecular Chemistry, Materials and Catalysis (MOST), Place Louis Pasteur 1, bte L4.01.02, 1348 Louvain-la-Neuve, Belgium

[2]Department of Chemistry, University of North Carolina at Chapel Hill, Chapel Hill, North Carolina, 27599-3290, United States

[3]Department of Chemistry and Pharmacy, Interdisciplinary Center for Molecular Materials (ICMM), Friedrich-Alexander-Universität Erlangen-Nürnberg, Egerlandstr. 3, 91058 Erlangen, Germany

[4]Universidad de Buenos Aires, Facultad de Ciencias Exactas y Naturales, Departamento de Química Inorgánica, Analítica y Química Física, Pabellón 2, Ciudad Universitaria, C1428EHA, Buenos Aires, Argentina.

[5]CONICET – Universidad de Buenos Aires. Instituto de Química Física de Materiales, Medio Ambiente y Energía (INQUIMAE), Pabellón 2, Ciudad Universitaria, C1428EHA, Buenos Aires, Argentina

[6]Spectroscopy, Quantum Chemistry and Atmospheric Remote Sensing (CP 160/09), Université libre de Bruxelles, 50 av. F. D. Roosevelt, B-1050 Brussels, Belgium

[7]Chemistry Division, Brookhaven National Laboratory, Upton, NY 11973-5000, USA

[8]Laboratoire de Chimie Organique, Université libre de Bruxelles (ULB), CP 160/06, 50 avenue F.D. Roosevelt, 1050 Brussels, Belgium.

*Correspondence to: Ludovic.Troian.Gautier@ulb.be, benjamin.elias@uclouvain.be, renatons@bnl.gov, gjmeyer@email.unc.edu

Abstract: Efficient excited-state electron transfer between an iron(III) photosensitizer and organic electron donors was realized with green light irradiation. This advance was enabled by the use of the previously reported iron photosensitizer, $[Fe(phtmeimb)_2]^+$ (phtmeimb = {phenyl[tris(3-methyl-imidazolin-2-ylidene)]borate}, that exhibited long-lived and luminescent ligand-to-metal charge transfer (LMCT) excited states. A benchmark dehalogenation reaction was investigated with catalytic yields that exceed 90% and an enhanced stability relative to the prototypical photosensitizer $[Ru(bpy)_3]^{2+}$. The initial catalytic step is electron transfer from an amine to the photoexcited iron sensitizer that is shown to occur with a large cage-escape yield. For LMCT excited states, this reductive electron transfer is vectoral and may be a general advantage of Fe(III) photosensitizers. In-depth time-resolved spectroscopic methods, that include transient absorption characterization from the ultraviolet to the infrared regions, provided a quantitative description of the catalytic mechanism with associated rate constants and yields.

INTRODUCTION

The scarcity of 2nd and 3rd row transition metals such as ruthenium, iridium, rhodium or osmium, coupled with a global desire for sustainable chemistry has led to the resurgence of research centered on earth-abundant metal-based photosensitizers.[1-4] Several photosensitizers based on copper,[5-6] molybdenum,[7] nickel,[8-9] tungsten,[10-11] zirconium,[12-13] chromium,[14-16] cobalt[17-18] or iron[19-37] have recently been reported as promising candidates in cutting-edge research fields. In particular, luminescent complexes of iron are often considered a 'holy grail' because of iron's high abundance in the earth's crust, low toxicity, and low environmental impact. The prototypical Fe(II) complex, *i.e.* $[Fe(bpy)_3]^{2+}$, first synthesized about sixty years ago, possesses metal-to-ligand charge-transfer (MLCT) excited states with broad visible light absorption from 400 to 550 nm like its Ru(II) and Os(II) counterparts. However, whereas $[Ru(bpy)_3]^{2+*}$ exhibits a photoluminescent ^{3}MLCT excited-state with an ~ 1 microsecond lifetime, $[Fe(bpy)_3]^{2+*}$ is non-luminescent due to the presence of a high-spin metal-centered states that rapidly deactivate the MLCT state.[1, 25] In recent years, strategies to enhance the MLCT excited-state lifetime of iron complexes have emerged[1] and led to an increase from ~10 ps in 2013[27] to 528 ps[38] in 2018, with several gradual advances in between. Presently, the longest-lived ^{3}MLCT excited state for a Fe(II) photosensitizer is ~2-2.5 ns in acetonitrile, toluene or THF.[35] Strikingly, $[Fe(phtmeimb)_2]^+$ (**1**$^+$) (phtmeimb = {phenyl[tris(3-methyl-imidazolin-2-ylidene)]borate}, an Fe(III) based photosensitizer reported in 2019 by Wärnmark

et al., exhibits an unconventional, low-lying luminescent doublet Ligand-to-Metal Charge Transfer (^{2}LMCT) excited-state with a lifetime of ~2.2 ns in CH_3CN.[29]

Until recently, the short excited-state lifetimes have limited the development of iron photosensitizers for photoredox catalysis to only a few reported applications,[19, 39-43] and the mechanistic pathways for the photocatalytic processes often remain unknown. Most notable examples include the use of $[Fe(bpy)_3]^{2+}$ and $[Fe(phen)_3]^{2+}$ for the organocatalytic, enantioselective alkylation of aldehydes[42] or for the photochemical synthesis of carbazole.[43] Recently, McCusker *et al.* showed that the MC ligand-field states of $[Fe(tren(py)_3)]^{2+}$ ($tren(py)_3$ = tris(2-pyridyl-methylimino-ethyl)amine) undergo excited-state quenching with quinone electron acceptors in fluid solution.[19] In all but one of these studies, diffusional excited-state electron transfer was assumed without direct experimental proof. The exception is $\mathbf{1}^+$, where excited state electron transfer was unequivocally demonstrated.[29] However, the resulting charge-separated states were formed in very low yields (<0.05), which hinders their utility in photoredox catalysis.[29]

Here we show that the $\mathbf{1}^+$ undergoes excited-state electron transfer with high yields (0.36-0.63) of charge separated products. The kinetic rate constant for this excited-state reactivity is also shown to be very large, k_{et} = 2.3 x10^{10} $M^{-1}s^{-1}$, approaching a value expected for a diffusion limited reaction. The monoreduced $[Fe(phtmeimb)_2]$ (**1**) photoproduct efficiently dehalogenated 4-bromobenzyl-2-chloro-2-phenylacetate (**2a**),[44-45] a benchmark catalytic reaction reported by Stephenson *et al.*[44, 46] that has relevance to organic synthesis and environmental applications. Additional mechanistic insights were obtained by time-resolved infrared spectroscopy (TRIR), which yielded the rate constant for reduction of **2a** by the monoreduced iron complex as k_{et} = 1.6 x10^8 $M^{-1}s^{-1}$. The data establish ^{2}LMCT excited states of Fe(III) complexes as highly competent earth abundant photocatalysts that possess significant advantages over the more commonly utilized MLCT excited states.

RESULTS AND DISCUSSIONS

The synthesis of $\mathbf{1}^+$ (**Figure 1A**) was performed following established procedures, with average yields of 3%.[29, 47,48] This yield increased to 30% when freshly prepared LiHMDS was used instead of ^{t}BuOK as discussed in the Supporting Information. The UV-visible absorption and photoluminescence (PL) spectra of $\mathbf{1}^+$ in N,N-dimethylformamide (DMF), acetonitrile (CH_3CN), butyronitrile (BuCN), acetone, and dichloromethane (CH_2Cl_2) are represented in **Figure 1D**. The photoluminescence maximum (PL_{max}) was shown to redshift from 641 nm to 667 nm when the solvent polarity was increased from CH_2Cl_2 to DMF, whereas the absorption

features were largely insensitive to the solvent identity. In addition, the excited-state lifetime was only slightly impacted by the solvent with values ranging from 2.4 ns in CH_2Cl_2 to 1.7 ns in DMF. This short excited-state lifetime also precluded reaction with dissolved oxygen (**Figures S3-S4**).[29]

Excited-state reactivity was investigated between $\mathbf{1}^{+}$* and a series of ten electron donors (**Figure 1B**). The Stern-Volmer plots from PL quenching experiments were linear, consistent with a dynamic quenching mechanism (**Figure 1E-F** and **Figures S5-S9**). In all cases, the quenching rate constants were close to the expected diffusion limit, *i.e.* with quenching rate constants, k_q, that ranged (0.86-2.65) x 10^{10} $M^{-1}s^{-1}$ for TMB, DMA, DMT, TTA and MPA, and (0.03-1.89) x 10^{10} $M^{-1}s^{-1}$ for DIPEA, TEA, Pip and TEOA (**Table S4**). Excited-state quenching did not occur with 4-bromobenzyl-2-chloro-2-phenylacetate, **2a** (**Figure S10**).

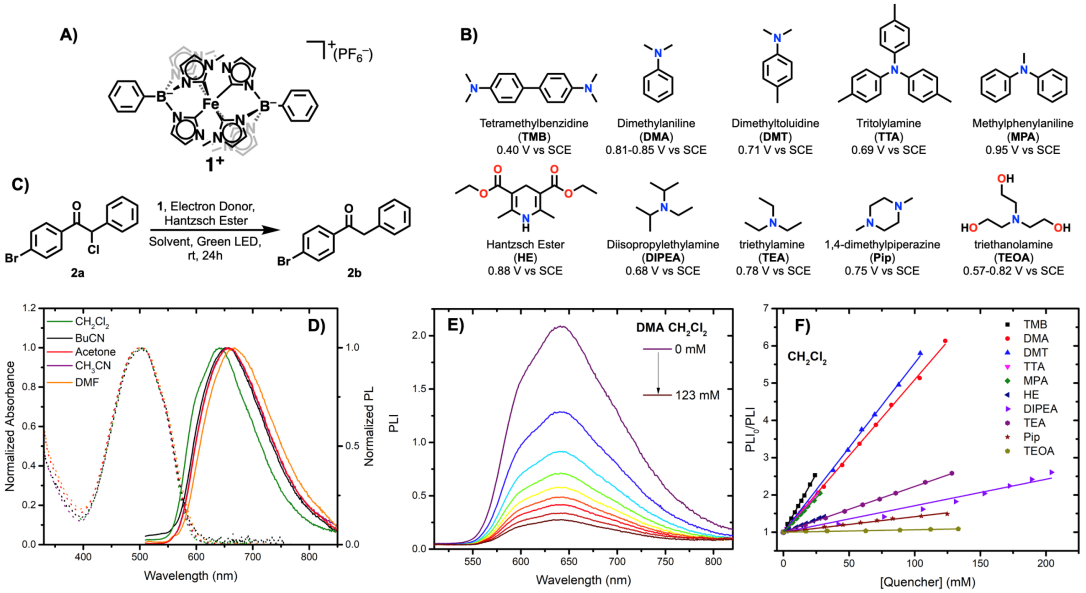

Figure 1. (**A**) Structure of $[Fe(phtmeimb)_2]^{+}.PF_6^{-}$, $\mathbf{1}^{+}$ and (**B**) the series of electron donors with their corresponding one-electron potentials *vs* SCE *i.e.* N,N,N',N'-tetramethylbenzidine (TMB), N,N-dimethylaniline (DMA), N,N-dimethyl-*p*-toluidine (DMT), tri-*p*-tolylamine (TTA), N-methyl-N-phenylaniline (MPA), N,N-diisopropylethylamine (DIPEA), triethylamine (TEA), 1,4-dimethylpiperazine (Pip), triethanolamine (TEOA) and diethyl-1,4-dihydro-2,6-dimethyl-3,5-pyridinedicarboxylate (Hantzsch ester, HE). (**C**) The investigated dehalogenation reaction. (**D**) Absorption and photoluminescence spectra of $\mathbf{1}^{+}$ in BuCN (black), DMF (orange), CH_2Cl_2 (green), acetone (red) and CH_3CN (purple). (**E**) A representative PL quenching experiment of $\mathbf{1}^{+*}$ with DMA in CH_2Cl_2 at RT. (**F**) Stern-Volmer plots in CH_2Cl_2 with all quenchers investigated. Additional Stern-Volmer plots in BuCN, DMF, acetone and CH_3CN can be found in the supporting information. All experiments were carried out at room temperature. UV-Vis absorption and PL spectra in CH_3CN are identical to those previously reported.[29] Redox potentials for the different electron donors were accessible in the literature.[49-55]

Nanosecond transient absorption spectroscopy (nsTAS) experiments were carried out to understand the origin(s) of the excited-state quenching. Spectral modelling of the transient absorption spectra measured after nanosecond pulsed 532nm laser excitation of $\mathbf{1}^{+}$ in a CH_2Cl_2 solution containing TTA, DMA or DMT (**Figure 2A**) was consistent with equimolar formation

of mono-reduced **1** and the respective oxidized electron donor. Hence the data is consistent with light absorption instigated electron transfer from the amine to $\mathbf{1}^{+*}$; a process often called reductive quenching that has previously been hypothesized for other Fe-based photocatalysts.[56] It is well known in photochemistry that, even when nearly 100% of the excited states are quenched, the yield of solvated charge-separated products can be small due to rapid back electron transfer within the solvent cage.[57-58] Here, the yields of products that escape the solvent cage, $\phi_{CE,}$ were determined in CH_2Cl_2, CH_3CN and DMF 100 ns after pulsed light excitation (**Figure 2b** and **Table 1**). These yields are shown to influence the overall catalytic efficiencies of visible light mediated chemical dehalogenation transformations.

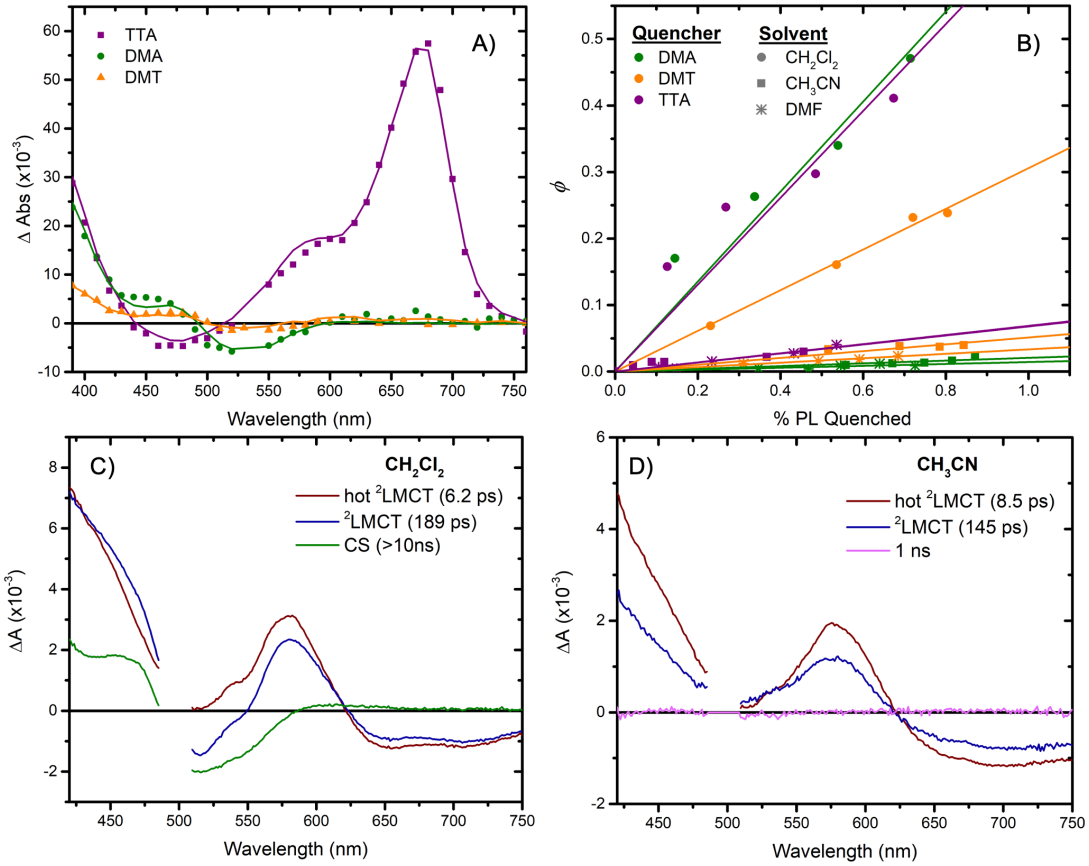

Figure 2. (**A**) Nanosecond transient absorption changes recorded under argon after pulsed 532 nm laser excitation (0.2 mM of $\mathbf{1}^{+}$, 200 mM of the indicated quencher in CH_2Cl_2). Absorption changes were modelled (solid line) as a 1:1 sum of the delta spectra of reduced **1** and oxidized quencher obtained by spectroelectrochemistry (see SI). (**B**) Cage-escape yields for DMA (green), DMT (orange) and TTA (purple) in CH_2Cl_2 (circle), CH_3CN (square) and DMF (crossed square) **(see supporting information for experimental details)**. (**C**-**D**) Femtosecond transient absorption changes recorded under argon after pulsed 500 nm laser excitation of $\mathbf{1}^{+}$ in the presence of 0.35M DMA in CH_2Cl_2 (**C**) and in CH_3CN (**D**).

Table 1. Cage escape yields determined by comparative actinometry in DMF, CH_3CN and CH_2Cl_2.

	[Fe(phtmeimb)$_2$]$^+$		
	CH_2Cl_2	CH_3CN	DMF
DMT	0.36 ±0.10	0.05 ±0.01	0.03 ±0.001
DMA	0.60 ±0.09	0.02 ±0.005	0.01 ±0.002
TTA	0.63 ±0.08	0.07 ±0.01	0.07 ±0.004

The cage escape yields measured by comparative actinometry in DMF and CH_3CN were less than 0.07 but reached much higher values (between 0.36 and 0.63) in CH_2Cl_2 (**Table 1** and **Figures S11-S13**). This occurred despite very similar excited-state quenching rate constants in all three solvents. The low photo-product yields observed in CH_3CN were consistent with a report by Wärnmark *et al.* who determined $\phi_{CE} = 0.05$ for both a N-phenylaniline electron donor and a methyl-viologen electron acceptor in CH_3CN.[29] Our results were also consistent with those reported by Persson *et al.*, who showed that electron transfer between DMA and $\mathbf{1}^{+*}$ only resulted in observable photoproducts at very large (> 500 mM) DMA concentrations, behavior attributed to ultrafast spin-allowed geminate charge recombination between reduced **1** and oxidized DMA (~0.2 ps^{-1}).[22] Hence, the large photoproduct yields in CH_2Cl_2 imply a dramatic decrease in the rate constant for geminate charge recombination within the solvent cage.

To test whether such putative ultrafast geminate recombination could be time-resolved, femtosecond transient absorption spectroscopy (fsTAS) was performed in CH_3CN and CH_2Cl_2 using DMA as the electron donor (**Figure 2C-D** and **Figures S15-S23**). fsTAS in CH_2Cl_2 clearly showed that the decay of LMCT excited states goes hand in hand with the formation of charge-separated (CS) states, unambiguously confirming that the dominant excited state quenching process is an electron transfer reaction from the amine to $\mathbf{1}^{+*}$. The spectral signatures of CS states matched those observed by nsTAS. Additionally, LMCT lifetimes derived from fsTAS afforded the corresponding electron transfer rate constant, k_{et} = 2.3 x10^{10} $M^{-1}s^{-1}$ that agreed with the rate constant obtained from PL quenching experiments. In stark contrast, no such state was observed in fsTAS in CH_3CN. This is consistent with the low yield of charge-separated products measured on the nanosecond time scale.

The fundamental factors that impact the measured cage escape yields in this study are unknown. In fact, the factors that impact cage escape yields are poorly understood in all of photochemistry, with electron spin being the only factor that has clearly been shown to have an impact.[57, 59-66] Indeed, the high ϕ_{CE} values in CH_2Cl_2 with an iron photocatalyst is surprising and rare in photochemistry. Furthermore, literature reports have shown a lower ϕ_{CE} in CH_2Cl_2 compared to CH_3CN or DMF for other photocatalysts. [44,63]

There are three plausible, yet speculative, hypotheses for the large cage escape yields observed with this iron photocatalyst. First, the ^{2}LMCT character of $\mathbf{1}^{+*}$ leads to a mono-reduced complex with a reduced iron (II) metal center. This is unlike prototypical MLCT excited states where the reduced photocatalyst has an electron localized on a bipyridine ligand.[67-70] Hence reductive quenching of an LMCT excited state results in vectoral electron transfer away from the donor, a process desired for applications in photoredox chemistry and solar energy conversion. In contrast, reductive quenching of an MLCT excited state results in non-vectoral electron transfer that leaves a ligand-localized electron proximate to the electron donor, which may promote strong electronic coupling and enhance charge recombination. Charge recombination after LMCT electron transfer from the metal center in mono-reduced **1**, however, requires electron tunneling through the ligands. This suggests that geminate charge recombination from mono-reduced **1** may be slowed relative to other common Fe photocatalysts such as $[Fe(bpy)_3]^{2+}$.

Second, $\mathbf{1}^+$ has an octahedral geometry in the ground state[29] with a d^5 ground state associated with a $^2T_2$ configuration of the iron(III). After excited state electron transfer, a d^6 low-spin iron(II) state with a $^1A_1$ configuration is obtained. These spin states are markedly different from that of the prototypical $[Ru(bpy)_3]^{2+}$, which is rigorously diamagnetic in the ground state and exhibits a ^{3}MLCT excited state with a distorted octahedral geometry that possesses a single reduced 2,2'-bipyridine ligand.[67-68, 71-73] Charge recombination for this prototypical ^{3}MLCT[60, 74-75] thus involves a spin-forbidden ^{3}CS → ^{1}GS electron transfer, very different from the spin-allowed ^{2}CS → ^{2}GS charge recombination of the ^{2}LMCT iron(III) photosensitizer **1** (**Figure 3**). These spin states might be expected to result in distinct solvent effects on cage escape yields. For example, cage escape yields after $[Ru(bpy)_3]^{2+*}$ to methyl viologen electron transfer have been reported to decrease in the presence of halogenated solvents or additives; behavior attributed to heavy atom promoted mixing of the ^{3}CS with lower spin states to attenuate the spin-forbidden character of charge recombination.[60] Herein, for the ^{2}CS of mono-reduced **1**, heavy atom effects in CH_2Cl_2 may similarly result in state mixing with a higher spin state such as the ^{4}CS (**Figure 3**). This would convey a partial spin-forbidden character to geminate charge recombination, slowing it down and thus increasing cage escape yields as was observed experimentally.

To further substantiate the heavy-atom effect on state-mixing, cage-escape yields were also determined in CH_2Br_2 and in acetonitrile:iodomethane mixtures (**Table 2**) of various ratios, as iodomethane is a common additive introduced to favor excited-state intersystem crossing.[60, 76-79] The cage-escape yields determined in CH_2Br_2 and CH_2Cl_2 were equal within experimental

error (**Figure 4a**). This is evident as the change in absorption at this observation wavelength is directly proportional to the yield of long-lived charge separated products. Furthermore, the addition of iodomethane into a solution of acetonitrile led to a ~5 fold gradual increase of cage-escape yields (**Figure 4b**), that increased from $\phi_{CE} = 0.02$ to $\phi_{CE} = 0.09$ (**Table 2**). Noteworthy is the fact that the cage-escape yields in these CH_3CN/MeI mixtures never reached values as high as those reported in CH_2Br_2 and CH_2Cl_2, suggesting that state-mixing might not be the sole contributor to these large cage-escape yields.

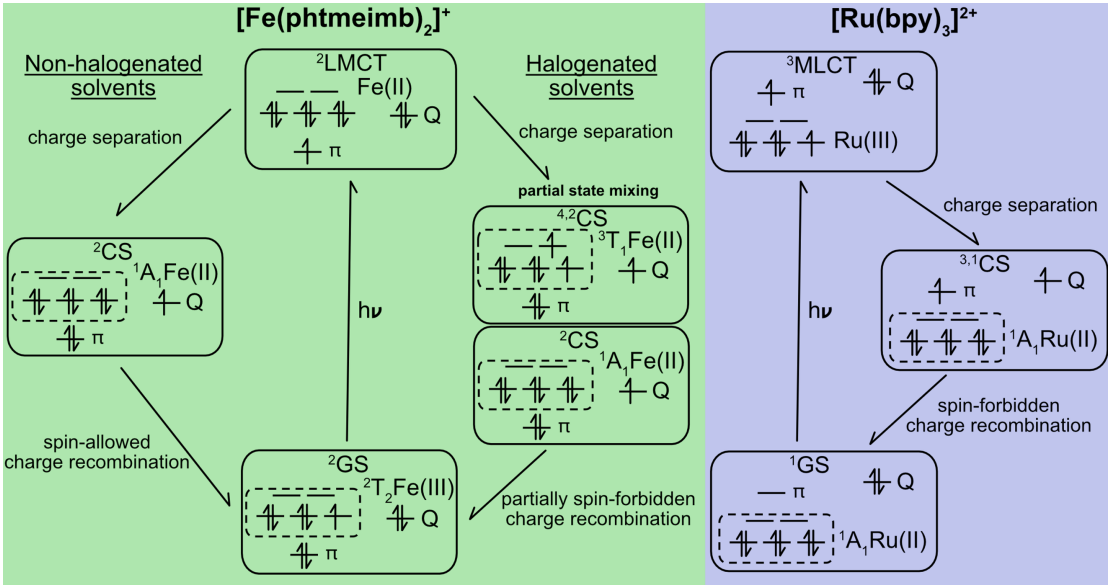

Figure 3. Schematic representation of the light-induced electronic transition involving iron(III) based LMCT photosensitizers (left), and ruthenium(II) based MLCT photosensitizers (right), together with an electron donor quencher (Q).

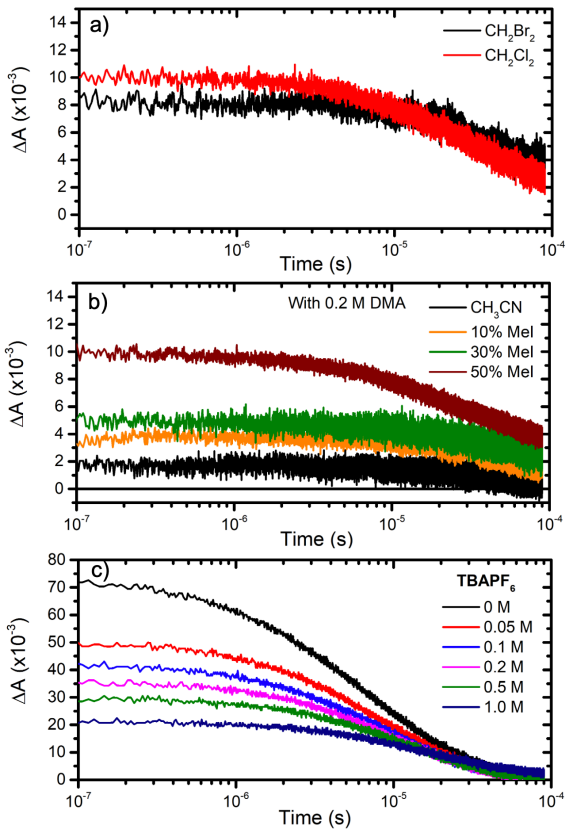

Figure 4. Nanosecond transient absorption changes recorded at 370 nm following pulsed light excitation of a solution of $\mathbf{1}^+$ and DMA in (a) CH_2Cl_2 and CH_2Br_2, (b) CH_3CN containing the indicated percentage of iodomethane and (c) CH_3CN containing the indicated concentration of $TBAPF_6$.

Table 2. Electrolyte and heavy atom effect of cage escape yields.

Conditions	ϕ_{CE}
CH_2Cl_2	0.60
CH_2Br_2	0.54
CH_3CN	0.02
CH_3CN + 30% MeI	0.05
CH_3CN + 50% MeI	0.09
CH_2Cl_2/$TBAPF_6$ (0.1M)	0.35
CH_2Cl_2/$TBAPF_6$ (0.2M)	0.30
CH_2Cl_2/$TBAPF_6$ (1M)	0.17

The high cage escape yields in CH_2Cl_2 and CH_2Br_2 may also result from the small dielectric constants of the solvents, 9.1 and 7.8 respectively, which may enhance electrostatic incentives for cage escape. The excited state electron transfer is termed a "charge-shift reaction" in which both the reactants and products have a total plus one charge and hence no net Coulombic work term contribution is expected.[80-81] Polarization, however, may play an

important role in the structure of the solvent cage before and after electron transfer. To further probe this idea, the geometry of the encounter complex after electron transfer was optimized by DFT using the 6-311G(d) basis set in the gas phase, CH_2Cl_2, CH_3CN, and DMF. The interaction energy, defined as the energy difference between the contact {**1**$^{-}$;DMA^{+}} and the fully solvated charge-separated species, were determined to be similar in CH_3CN (–48.5 kcal/mol) and CH_2Cl_2 (–50.0 kcal/mol). Nevertheless, the partial atomic charges of the reduced photosensitizer and oxidized electron donor were separately optimized in CH_2Cl_2, CH_3CN and DMF. In the low dielectric CH_2Cl_2, this natural bond order analysis revealed that both the reduced photocatalyst and the oxidized electron donor were polarized with net positively charged repulsive regions that create an electric field that would assist separation of the electron transfer products (**Figure 5** and **Figures S37-S40**). This field was almost entirely screened in polar solvents, such as in CH_3CN or DMF, consistent with the smaller cage escape yield measured experimentally. Hence this electrostatic repulsion predicts that a lower dielectric constant environment will favor cage escape yields between **1** and $DMA^{\bullet+}$. This hypothesis is further supported by experiments that showed that ϕ_{CE} decreased by ~70% in CH_2Cl_2 (from ϕ_{CE} = 0.60 to ϕ_{CE} = 0.17) when the ionic strength was increased by the addition of 1.0 M tetrabutylammonium hexafluorophosphate ($TBAPF_6$) (**Table 2**) (**Figure 4c**).

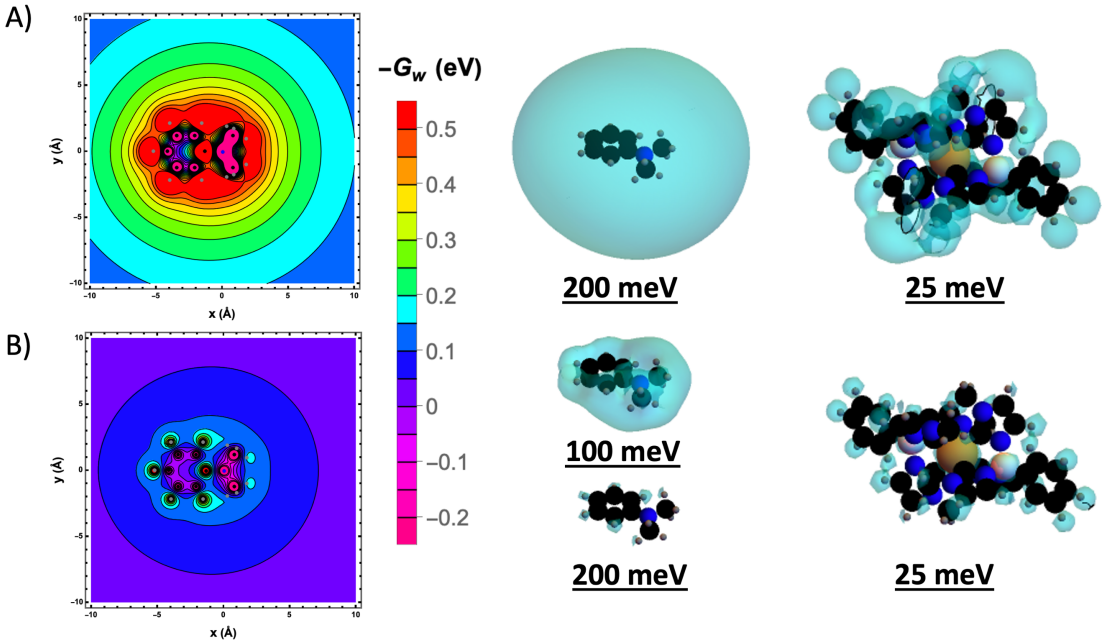

Figure 5. 2D contour plot (left) for the coulombic repulsion of DMA^{+} with a spherical cation (+1 charge) in CH_2Cl_2 (A) and CH_3CN (B). The right-hand side shows the three-dimensional contour diagrams for DMA^{+} or mono-reduced **1** plotted at the indicated potential. Therefore, the three-dimensional contour diagrams at 200 meV indicates the relative distance at which a repulsion of 200 meV is exerted on an approaching cation (+1 charge). Plots in DMF are shown in **figure S40**.

Photoredox catalysis and time-resolved infrared spectroscopy

The transient absorption data indicates that the visible light mediated dehalogenation catalysis would proceed with higher yields in dichloromethane compared to solvents of higher polarity. Indeed, 90% conversion of **2a** into **2b** was realized after 24 hours in CH_2Cl_2 solutions with ~ 0.35 M DMA and 1 mol% of $\mathbf{1}^+$, with excellent isolated yields (**Table 3**, **entry 1-6**). The yields did indeed decrease significantly to 15%, 7%, 30% and 31%, in acetone, BuCN, CH_3CN or DMF, respectively (**Table S1, Entry 1-4**).

Control experiments highlighted that DMA was needed to obtain a large reaction yield as the yield dropped from 87% to 39% in the absence of DMA (**Table 3**, **entries 4 and 10**). Hantzsch ester (HE in **Figure 1**) could also trigger the reduction of $\mathbf{1}^{+*}$ (**Table 3**, **entry 10-11**), as further evidenced by the quenching rate constant of 0.56 x 10^{10} $M^{-1}s^{-1}$ in CH_2Cl_2. Under otherwise identical conditions, $[Fe(bpy)_3]^{2+}$ did not yield any dehalogenation product (**Table 3**, **entry 14**), whereas $[Ru(bpy)_3]^{2+}$ was competent for light-induced dehalogenation with a 94% isolated yield (**Table 3**, **entry 13**). However, after reaction with $[Ru(bpy)_3]^{2+}$, the orange solution turned purple which is a clear indication of ligand-loss chemistry and hence photosensitizer degradation that is obviously problematic for mechanistic investigations and, more importantly, for catalyst recyclability. On the contrary, when the iron photosensitizer $\mathbf{1}^+$ was used, the solution absorbance was unchanged over the course of the reaction, indicative of photosensitizer integrity, which could be recovered with 88% yield after photoreaction. Photoreactions performed with recycled $\mathbf{1}^+$ led to dehalogenation of **2a** to **2b** with unaltered yields. Finally, a reaction quantum yield of 0.0020% on an absorbed photon basis was determined for the green-light mediated dehalogenation reaction of **2a** to **2b** using 1mol% of $\mathbf{1}^+$, 0.35M of DMA and 1.5 eq of HE.

The yield of the dehalogenation reaction was dependent on the nature of the electron donor. Tertiary aromatic amines, such as TMB, TTA and MPA gave larger quenching rate constants than other amines. Nevertheless, the net dehalogenation reaction was inefficient with these quenchers, with yields of **2b** ranging from 2% for TMB and TTA to 13% for MPA (**Table S2, Entry 1-3**). In contrast, sacrificial electron donors, which promote irreversible reactions, such as DIPEA, TEA, N,N'-Me_2-piperazine and DMT led to light-induced dehalogenation with yields ranging from 85% (1,4-dimethylpiperazine) to 95% (TEA) (**Table 4**). The experiments performed with 1,4-dimethylpiperazine also pointed towards the influence of viscosity on the dehalogenation yields (**Table 4, entry 9-10**). Yields of 85% were obtained when 0.35 M of 1,4-dimethylpiperazine was used and dropped to 47% when the concentration was increased to 2

M, *i.e.* a concentration at which the bulk viscosity was considerably modified. On the other hand, yields were almost unchanged when the concentration of TEA ranged from 0.35 M to 1.17 M (**Table 4, entry 6-7**). This is directly related to the increased viscosity of 1,4-dimethylpiperazine (1.5 cP at 20°C) compared to TEA (0.36 cP at 20°C) that alters diffusion and probably favors geminate charge-recombination.[82-85]

The low yields observed with reversible electron donor most likely originate from recombination of the oxidized amine with the reduced photocatalyst.[86] Nanosecond transient absorption revealed that back electron transfer occurred on a faster timescale with reversible electron donor compared to sacrificial electron donor (**Figure S14**). In addition, the initial baseline was not fully recovered when TEA was used, indicative of accumulation of mono-reduced **1** via the degradation of TEA, hence preventing any back electron transfer process.

Interestingly, with TEA and DIPEA, the use of Hantzsch Ester helped to obtain higher dehalogenation yields (**Table 4 entry 2 and 6**) but was not mandatory as yields > 90% with TEA were obtained in the absence of Hantzsch Ester when large TEA concentrations were employed (**Table 4 entry 7**). This indicates that triethylamine first acts as electron donor, leading to the corresponding oxidized radical cation that can in turn undergo hydrogen atom transfer to form the iminium,[87] alleviating the need of HAT reagents such as Hantzsch Ester.

A prototypical reaction in CD_2Cl_2 with green light irradiation was monitored by ^1H NMR spectroscopy at regular time intervals (**Figure S29**). It was shown that the substrate underwent full dehalogenation, as shown by the total conversion of one singlet at 5.38 ppm to a singlet at 5.07 ppm. In addition, the Hantzsch Ester was also shown to undergo reaction chemistry, probably through H atom transfer, as the aromatized pyridine core was recovered and isolated at the end of the reaction. Note that HE was consumed more rapidly when DMA was used as electron donor compared to TEA, in which case some unreacted HE was still present at the end of the reaction.

Table 3. Control experiments and optimization of the visible-light mediated dehalogenation reaction of **2a** in **2b** using DMA and Hantzsch Ester (HE).

Entry	Conditions	Lamp	Conversion	Yield
1	$\mathbf{1}^+$ (2.5 mol%), **2a** (0.2mmol), **DMA (0.5M**, 1 mmol, 5.0 eq**)**, HE (0.3 mmol, 1.5 eq), CH_2Cl_2, 24h	Green	98%	95%
2	$\mathbf{1}^+$ (2.5 mol%), **2a** (0.2mmol), **DMA (0.35M**, 0.7 mmol, 3.5 eq**)**, HE (0.3 mmol, 1.5 eq), CH_2Cl_2, 24h	Green	97%	94%
3	$\mathbf{1}^+$ (2.5 mol%), **2a** (0.2mmol), **DMA (0.2M**, 0.4 mmol, 2.0 eq**)**, HE (0.3 mmol, 1.5 eq), CH_2Cl_2, 24h	Green	88%	86%
4	$\mathbf{1}^+$ **(1 mol%)**, **2a** (0.2mmol), DMA (0.35M, 0.7 mmol, 3.5 eq), HE (0.3 mmol, 1.5 eq), CH_2Cl_2, 24h	Green	90%	87%
5	$\mathbf{1}^+$ (1 mol%), **2a** (0.2mmol), DMA (0.35M, 0.7 mmol, 3.5 eq), HE (0.3 mmol, 1.5 eq), CH_2Cl_2, **12h**	Green	64%	57%

6	$\mathbf{1}^+$ (1 mol%), **2a** (0.2mmol), DMA (0.35M, 0.7 mmol, 3.5 eq), HE (0.3 mmol, 1.5 eq), CH_2Cl_2, **16h**	Green	82%	78%
7	$\mathbf{1}^+$ (1 mol%), **2a** (0.2mmol), DMA (0.35M, 0.7 mmol, 3.5 eq), HE (0.3 mmol, 1.5 eq), CH_2Cl_2, 24h	Blue	52%	41%
8	$\mathbf{1}^+$ (1 mol%), **2a** (0.2mmol), DMA (0.35M, 0.7 mmol, 3.5 eq), HE (0.3 mmol, 1.5 eq), CH_2Cl_2, 24h	Orange	68%	60%
9	$\mathbf{1}^+$ (1 mol%), **2a** (0.2mmol), DMA (0.35M, 0.7 mmol, 3.5 eq), HE (0.3 mmol, 1.5 eq), CH_2Cl_2, 24h	White	75%	69%
10	$\mathbf{1}^+$ (1 mol%), **2a** (0.2mmol), **No DMA**, HE (0.3 mmol, 1.5 eq), CH_2Cl_2, 24h	Green	46%	39%
11	$\mathbf{1}^+$ (1 mol%), **2a** (0.2mmol), **No DMA**, HE (0.5 mmol, **2.5 eq**), CH_2Cl_2, 24h	Green	61%	48%
12	$\mathbf{1}^+$ (1 mol%), **2a** (0.2mmol), DMA (0.35M, 0.7 mmol, 3.5 eq), **No HE**, CH_2Cl_2, 24h	Green	9%	2%
13	$Ru(bpy)_3(PF_6)_2$ (1 mol%), **2a** (0.2mmol), DMA (0.35M, 0.7 mmol, 3.5 eq), HE (0.3 mmol, 1.5 eq), CH_2Cl_2, 24h	Blue	100%	94%
14	$Fe(bpy)_3(Br)_2$ (1 mol%), **2a** (0.2mmol), DMA (0.35M, 0.7 mmol, 3.5 eq), HE (0.3 mmol, 1.5 eq), CH_2Cl_2, 24h	Green	8%	1%
15	**No PS**, **2a** (0.2mmol), DMA (0.35M, 0.7 mmol, 3.5 eq), HE (0.3 mmol, 1.5 eq), CH_2Cl_2, 24h	Green	6%	3%
16	1^+ (1 mol%), **2a** (0.2mmol), DMA (0.35M, 0.7 mmol, 3.5 eq), HE (0.3 mmol, 1.5 eq), CH_2Cl_2, one hour illumination and 24h in dark	Green	26%	15%
17	1^+ (1 mol%), **2a** (0.2mmol), DMA (0.35M, 0.7 mmol, 3.5 eq), HE (0.3 mmol, 1.5 eq), CH_2Cl_2, 24h, carried out under air	Green	57%	55%

Table 4. Optimization of the visible-light mediated dehalogenation reaction of **2a** in **2b** using DIPEA, TEA, DMT and 1,4-dimethylpiperazine (pip) as electron donor.

Entry	Conditions	Lamp	Conversion	Yield
1	$\mathbf{1}^+$ (1 mol%), **2a** (0.2mmol), DIPEA (2 M, 4 mmol, 20 eq), HE (0.3 mmol, 1.5 eq), CH_2Cl_2, 24h	Green	89%	90%
2	$\mathbf{1}^+$ (1 mol%), **2a** (0.2mmol), DIPEA (0.35 M, 0.7 mmol, 3.5 eq), HE (0.3 mmol, 1.5 eq), CH_2Cl_2, 24h	Green	97%	89%
3	$\mathbf{1}^+$ (1 mol%), **2a** (0.2mmol), DIPEA (0.35 M, 0.7 mmol, 3.5 eq), **No HE**, CH_2Cl_2, 24h	Green	66%	63%
4	$\mathbf{1}^+$ (1 mol%), **2a** (0.2mmol), DIPEA (2 M, 4 mmol, 20 eq), **No HE**, CH_2Cl_2, 24h	Green	77%	75%
5	$\mathbf{1}^+$ (1 mol%), **2a** (0.2mmol), TEA (1.17 M, 2.3 mmol, 11.7 eq), HE (0.3 mmol, 1.5 eq), CH_2Cl_2, 24h	Green	100%	95%
6	$\mathbf{1}^+$ (1 mol%), **2a** (0.2mmol), TEA (0.35 M, 0.7 mmol, 3.5 eq), HE (0.3 mmol, 1.5 eq), CH_2Cl_2, 24h	Green	96%	89%
7	$\mathbf{1}^+$ (1 mol%), **2a** (0.2mmol), TEA (1.17 M, 2.3 mmol, 11.7 eq), **No HE**, CH_2Cl_2, 24h	Green	94%	94%
8	$\mathbf{1}^+$ **(1 mol%)**, **2a** (0.2mmol), DMT (0.35M, 0.7 mmol, 3.5 eq), HE (0.3 mmol, 1.5 eq), CH_2Cl_2, 24h	Green	93%	86%
9	$\mathbf{1}^+$ **(1 mol%)**, **2a** (0.2mmol), Pip (2 M, 4 mmol, 20 eq), HE (0.3 mmol, 1.5 eq), CH_2Cl_2, 24h	Green	57%	47%
10	$\mathbf{1}^+$ **(1 mol%)**, **2a** (0.2mmol), Pip (0.35 M, 0.7 mmol, 3.5 eq), HE (0.3 mmol, 1.5 eq), CH_2Cl_2, 24h	Green	87%	85%

Time-resolved infrared (TRIR) spectroscopy was implemented to obtain structural information, with sub-microsecond kinetic resolution of the reactants and transient radical intermediates following pulse light excitation of $\mathbf{1}^+$.[88] Note that the reaction involving DMA

and HE could be monitored by TRIR whereas the one using TEA could not. This is due to a combination of the short excited-state lifetime of $\mathbf{1}^{+*}$ as well as the moderate cage-escape yields obtained with TEA (0.21 ±0.05) compared to the one determined with DMA (0.60 ±0.09). The results, gathered in **Figure 6**, in addition to the previously described experiments, provided an in-depth understanding of the overall mechanism for the photoredox catalytic transformations. This reaction mechanism was studied with TEA as sacrificial electron donor (**Figure 7A**), however attempts to interrogate the underlying mechanisms through time resolved spectroscopies were frustrated by low cage escape yields. As a result, key reaction details could not be experimentally determined with TEA as a sacrificial reagent. In contrast, the use of DMA and the Hantzsch Ester (**Figure 7B**) did provide mechanistic insights that are described below.

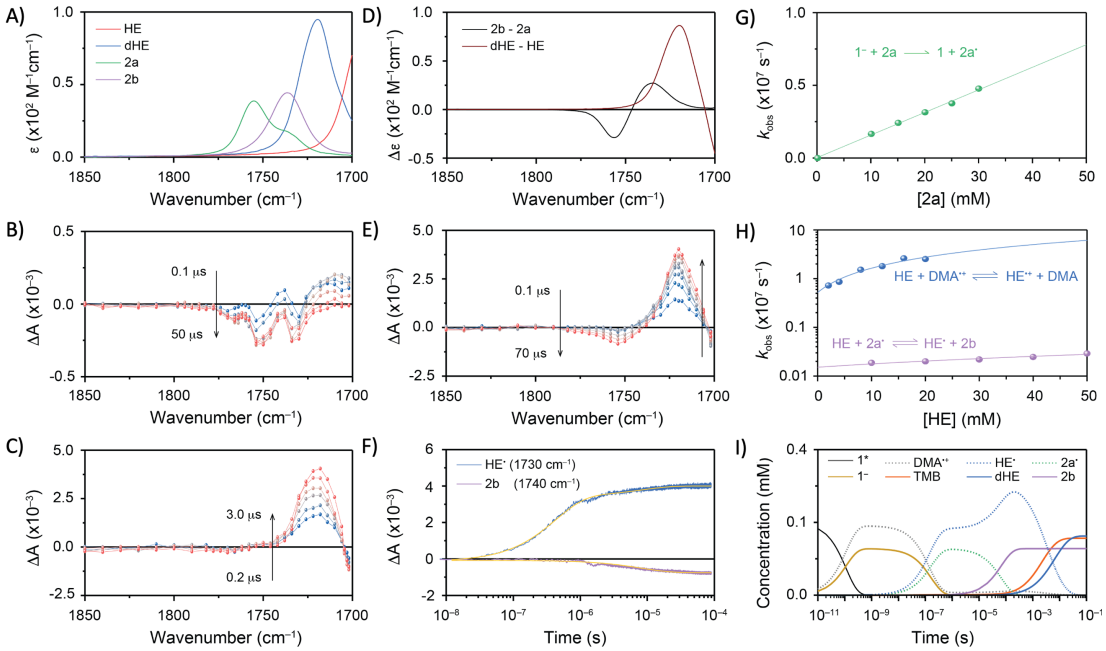

Figure 6. TRIR studies of the photo-initiated redox reactions. (**A**) Fourier transform infrared (FTIR) spectra of the relevant substrates (an extended FTIR spectra is available in **Figure S34**). TRIR absorption changes measured after a pulsed 500 nm laser excitation of solution mixtures containing (**B**) [$\mathbf{1}^{+}$] = 3 mM, [DMA] = 1 M, [2a] = 30 mM; and (**C**) [$\mathbf{1}^{+}$] = 3 mM, [DMA] = 1 M, [HE] = 30 mM. (**D**) Differential absorption changes expected for substrate transformations 2b ⟶ 2a and dHE ⟶ HE. (**E**) TRIR absorption changes measured after a pulsed 500 nm laser excitation of a solution mixture containing [$\mathbf{1}^{+}$] = 3 mM, [DMA] = 1 M, [HE] = 30 mM, [2a] = 30 mM. (**F**) Kinetic traces measured at the indicated wavenumbers that report on HE$^{\bullet}$ and **2b** formations. (**G**, **H**) Plots of the measured kinetic rate constants as a function of the indicated substrate concentrations. Overlaid to experimental data points are linear fits from which second-order rate constants were extracted. I) Simulated time dependent concentrations of the indicated reaction components based on experimentally determined kinetic parameters (see supporting material).

Mechanistically, the excited state $\mathbf{1}^{+*}$ was reductively quenched via electron transfer (**step 1**) generating the monoreduced **1** and oxidized quencher in a 1:1 ratio. When DMA was used as quencher in experiments performed in CH_2Cl_2, about 60% of the photogenerated **1** resulted in productive charge shift, $\mathbf{1}^{+*}$ + DMA ⟶ **1** + DMA$^{\bullet+}$, as determined by the cage-escape

yield of 0.60 ±0.09. The mono-reduced **1** transfers an electron to **2a**, with a kinetic rate constant of 1.6 x 10^8 M^{-1} s^{-1}, which irreversibly induced heterolytic C–Cl bond breaking to yield the corresponding **2a**$^{\bullet}$ radical and (presumably) Cl^- (**Figure 6b** and **Figure S35**). DFT calculations indicated that the transferred electron populates the LUMO of **2a,** which is centered on the 2-chloro-2-phenylacetate backbone (**Figure 7**). In fact, the intrinsic molecular properties as described by atomic vectors generated from nuclear Fukui functions for **2a** and **2a**$^{\bullet}$ indicated that the fragmentation process – *dehalogenation* – occurs along the C–Cl bond axis (**Figure 7** and **Figure S36**).

The sacrificial behavior of DMA as an irreversible electron donor requires that a second DMA molecule deprotonate the aromatic carbon oriented *para* to the amine group of the oxidized DMA$^{\bullet+}$ to generate a DMA$^{\bullet}$ radical (**step 1** in **Figure 7**).[89-90] The subsequent encounter of two DMA$^{\bullet}$ radicals leads to dimerization and formation of TMB. This leak reaction ensures the sacrificial behavior of DMA as the electron donor. This dimerization reaction, studied in great detail by Bard *et al.*, occurs in CH_3CN with a rate constant of 2.5 x10^8 $M^{-1}s^{-1}$.[90] TRIR data revealed that HE and DMA$^{\bullet}$ also undergo side reactivity via hydrogen atom transfer (HAT). Although the absorption changes shown in **Figure 6c** were similar to those expected for the formation of dehydrogenated HE (dHE), kinetic analysis (**Figure S35)** suggested the existence of a reaction equilibrium HE + DMA$^{\bullet}$ ⇌ HE$^{\bullet}$ + DMA as evidenced by a non-zero intercept in the observed rates measured as a function of the HE concentration under pseudo-first order conditions. This leads to an unwanted consumption of HE that competes with the desired pathway for product formation. This finding agrees with ^{1}H NMR observations that revealed that an excess of HE was needed to ensure complete conversion of **2a** into **2b**.

TRIR experiments that emulate the photoredox catalysis conditions are shown in **Figures 6e** and **6f**. The absorption changes that follow pulsed light excitation showed biphasic kinetics centered around 1730 cm^{-1} indicating a sub-microsecond initial formation of HE$^{\bullet}$, most likely generated from reaction with DMA$^{\bullet}$. Reduction of **2a** by monoreduced **1** (**step 2**) is fast and generates **2a**$^{\bullet}$, which undergoes HAT with HE (**step 4**) in another reaction equilibrium, **2a**$^{\bullet}$ + HE ⇌ **2b** + HE$^{\bullet}$, with a rate constant that is slow compared to the other kinetic processes. The fact that **step 4** is an equilibrium indicates that dHE has not yet been formed on the hundreds of microsecond time scales and likely represents the rate determining step in the catalytic cycle. The irreversible dehydrogenation of HE$^{\bullet}$ to produce the more stable – by about 30 kcal mol^{-1} – dHE could not be fully elucidated from experimental data, and might indeed involve multiple and competitive reaction pathways. [91-96] For instance, hydrogen atom transfer from HE$^{\bullet}$ to **2a**$^{\bullet}$ is more favorable compared to HE due to the subsequent aromatization of the pyridine ring

forming dHE. However, such pathway would have produced near equimolar concentrations of **2b** and **dHE**. Though HE$^{\bullet}$ could be a stronger reductant than HE and could reductively quench the excited state of $\mathbf{1}^{+*}$, the minimal concentrations of HE$^{\bullet}$ photoproduced by light excitation is unlikely to compete kinetically with DMA, which is present at much larger concentrations. Direct electron transfer from HE$^{\bullet}$ to **2a** forming **2a**$^{\bullet}$ has some precedence from similar dehalogenation reactions using Ir-based photosensitizers, Hantzsch Ester and K_3PO_4,[97] but may not be significant to the catalytic scheme in **Figure 7** since the overall reaction proceeds efficiently in the absence of HE with TEA and DIPEA. Alternative proton-coupled electron transfer pathways involving DMA or other bases could be considered and will motivate future investigation.

The collective interpretation of the findings obtained from TRIR indicate that the overall photocatalytic process is dominated by two kinetically competing reaction equilibria (**steps 3** and **4**) that consume the same substrate, HE. Nevertheless, dimerization of two DMA$^{\bullet}$ to form TMB and conversion of HE$^{\bullet}$ to dHE are important irreversible processes that drive the equilibria in the catalytic cycle towards the desired **2b** as the final product.

The reaction dynamics of the photoredox catalytic cycle shown in **Figure 7** were simulated from numerical solutions of the coupled differential equations (**See Supporting Information**) that describe the time dependent concentrations of all reaction components. These simulations are shown in **Figure 6I** for the indicated reaction components. The biphasic formation of HE$^{\bullet}$, as described in **steps 3** and **4** of the cycle in **Figure 7**, is readily observed. The bimolecular and concentration dependent kinetics for consumption of HE$^{\bullet}$ and dimerization of DMA$^{\bullet+}$ largely control the final formation of dHE relative to **2b**. In fact, the kinetic analysis in **Figure 6I** shows that dHE is formed in excess of 1.3 times compared to **2b** – a result that compares well with steady-state photoreaction experiments that required excess amounts of HE to ensure complete conversion of **2a** to **2b**.

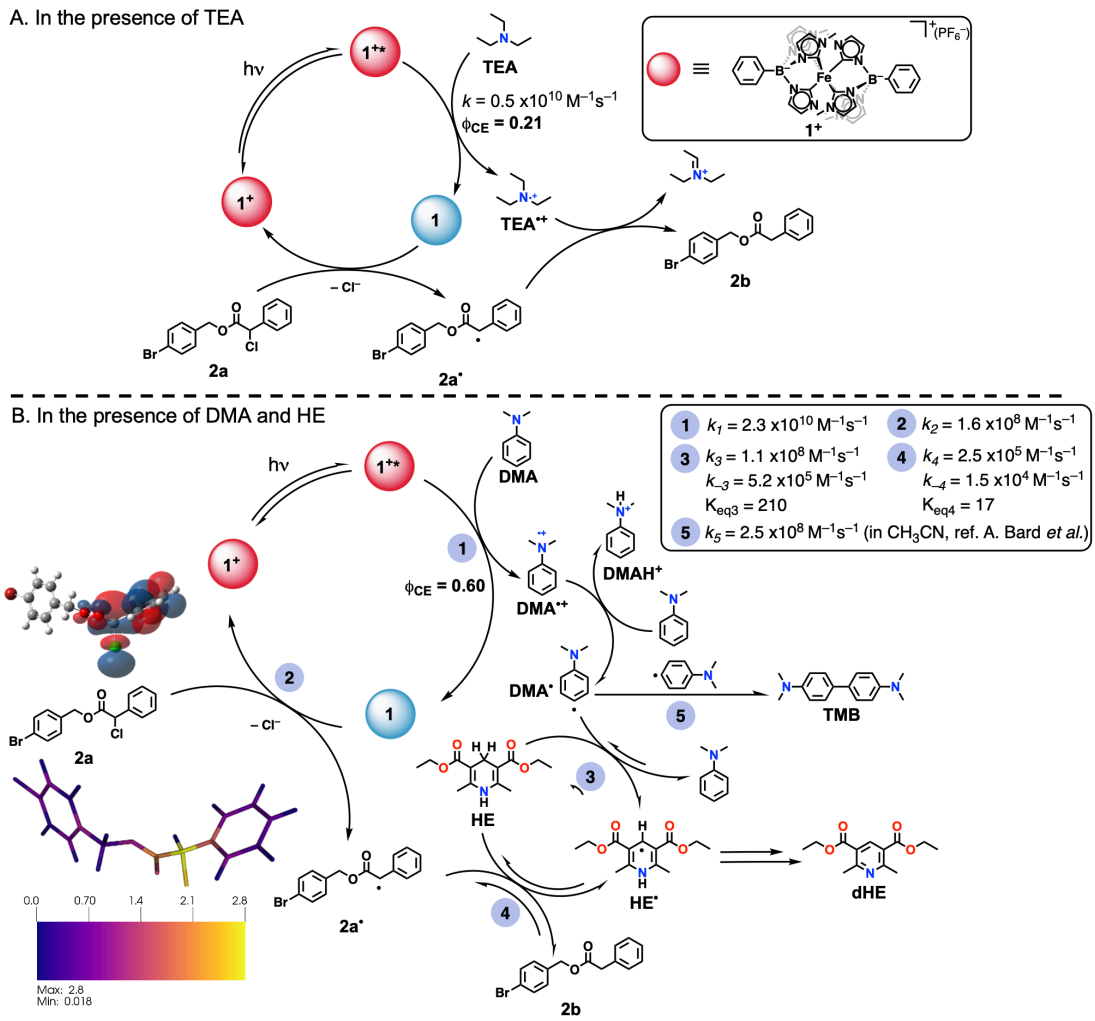

Figure 7. Proposed mechanism for the visible-light mediated dehalogenation of **2a** to **2b** in CH_2Cl_2 using $\mathbf{1}^+$ as photosensitizer in the presence of TEA as sacrificial electron donor (A) or in the presence of DMA as a sacrificial electron donor and HE (B). The LUMO of **2a** was calculated at the MP2 level using the 6-311G(g) basis. The magnitude of the nuclear Fukui functions (in eV/Å) (B3LYP/6-311G(d)) characterizing the changes in the force that the atoms experience following the electron-attachment in **2a** are represented on the lower left. See text for additional information regarding reaction steps and associated reaction rates.

CONCLUSIONS

The ~2 ns excited-state lifetime of an iron photocatalyst was optimized for a benchmark dehalogenation reaction that operated with yields greater than 90% with green light irradiation. The systematic variation of quenchers and solvents with mechanistic analysis allowed the key parameters that trigger this photoreactivity to be isolated. Sacrificial electron donors were found to be more optimal than reversible electron donors, which favored the formation of mono-reduced **1**, that was shown to reduce organic substrates. Although electron transfer was experimentally observed in CH_2Cl_2, CH_3CN and DMF, polar solvents such as DMF and CH_3CN did not lead to appreciable cage-escape yields (<0.07). On the contrary, CH_2Cl_2 afforded large

cage-escape yields (0.36-0.63), an observation that stands in contrast to the commonly expected behavior of MLCT and organic excited states where polar solvents favor cage escape. Three plausible hypotheses for the large cage-escape yields were proposed: the vectoral nature of reductive electron transfer with an LMCT excited state, an increased state-mixing due to the heavy-atom effect, and electrostatic repulsion between the reduced iron photosensitizer and the oxidized electron donor due to solvent dielectric effects. Experiments performed to probe the increased state-mixing (CH_2Br_2 or in CH_3CN/MeI mixtures) or the electrostatic repulsion (with added $TBAPF_6$) indicate that the large cage-escape yields originate from a combination of these two effects.

The reaction mechanism was investigated in molecular detail by nanosecond and femtosecond transient absorption as well as by time-resolved infrared spectroscopy. Reductive electron transfer between $\mathbf{1}^{+*}$ and DMA was experimentally confirmed, with k_{et} = 2.3 x10^{10} $M^{-1}s^{-1}$ generating **1** that could further reduce **2a**, with k = 1.6 x10^{8} $M^{-1}s^{-1}$. Radical intermediates that are often believed to be too short-lived and too reactive to allow for mechanistic investigations, were instead shown to participate in competing reaction equilibria (**steps 3** and **4**) that were responsible for Hantzsch ester consumption and provided additional insights into side reactions that occur with DMA but not with TEA, ultimately leading to more atom-economic transformation.

Collectively, the experimental and theoretical approaches described provide a clear description of the mechanistic intricacies that allow one to pin-point bottlenecks and pitfalls of photoredox catalysis with LMCT excited states that in turn should help improve visible-light mediated transformations with earth abundant photosensitizers.

ASSOCIATED CONTENT

Supporting Information: Materials, Experimental procedures, Photocatalysis results, Absorption spectra, Time-Corelated Single Photon Counting, Stern-Volmer experiments, Nanosecond and femtosecond transient absorption spectroscopy, spectroelectrochemistry, TRIR experiments and DFT calculations. This material is available free of charge on the ACS Publications website

AUTHOR INFORMATION

Corresponding Authors

Ludovic.Troian.Gautier@ulb.be, benjamin.elias@uclouvain.be, renatons@bnl.gov, gjmeyer@email.unc.edu

Author Contributions

The manuscript was written through contributions of all authors. All authors have given approval to the final version of the manuscript.

Funding Sources

No competing financial interests have been declared.

ACKNOWLEDGEMENTS

This work was carried out at the Université catholique de Louvain, the University of North Carolina at Chapel Hill, the Friedrich-Alexander-Universität Erlangen-Nürnberg, Brookhaven National Laboratory and the Université libre de Bruxelles. The Fonds National pour la Recherche Scientifique (F.R.S.-FNRS) is greatly acknowledged for an individual FRIA fellowship (A.A.), the Chargé de Recherches individual fellowship (L.T.-G.) and continuous support (B.E.) for support of the iron(III) photocatalyzed initial mechanistic studies. R.E.B., M.D.T., G.J.M., and D.T.C. acknowledge the Center for Hybrid Approaches in Solar Energy to Liquid Fuels, CHASE, an Energy Innovation Hub funded by the US Department of Energy, Office of Basic Energy Sciences, Office of Science, under award number DE-SC0021173, for support of the light-initiated mechanistic studies and HAT reactivity. Computational resources were provided by the Shared ICT Services Centre, Université libre de Bruxelles. A.C. acknowledges the Argentinian Logistic Network and Dirk M. Guldi for providing access to transient absorption spectroscopy facilities. The authors acknowledge the Engineering of Molecular NanoSystems (EMNS) for granting access to the Fluorolog instrument. Time-resolved Infrared experiments were performed (R.N.S.) in the laboratories of the Artificial Photosynthesis group at Brookhaven National Laboratory supported by the U.S. Department of Energy, Office of Science, Office of Basic Energy Sciences, Division of Chemical Sciences, Geosciences & Biosciences under contract no. DE-SC0012704.

REFERENCES

1. Wenger, O. S., Is Iron the New Ruthenium? *Chem-Eur. J.* **2019,** *25*, 6043-6052.
2. Wenger, O. S., Photoactive Complexes with Earth-Abundant Metals. *J. Am. Chem. Soc.* **2018,** *140*, 13522-13533.

3. Zhou, W.-J.; Wu, X.-D.; Miao, M.; Wang, Z.-H.; Chen, L.; Shan, S.-Y.; Cao, G.-M.; Yu, D.-G., Light Runs Across Iron Catalysts in Organic Transformations. *Chem-Eur. J.* **2020,** *26*, 15052-15064.
4. Abderrazak, Y.; Bhattacharyya, A.; Reiser, O., Visible-Light-Induced Homolysis of Earth-Abundant Metal-Substrate Complexes: A Complementary Activation Strategy in Photoredox Catalysis. *Angew. Chem. Int. Ed.* **2021**, doi.org/10.1002/anie.202100270
5. Cuttell, D. G.; Kuang, S.-M.; Fanwick, P. E.; McMillin, D. R.; Walton, R. A., Simple Cu(I) Complexes with Unprecedented Excited-State Lifetimes. *J. Am. Chem. Soc.* **2002,** *124*, 6-7.
6. Armaroli, N., Photoactive mono- and polynuclear Cu()–phenanthrolines. A viable alternative to Ru()–polypyridines? *Chem. Soc. Rev.* **2001,** *30*, 113-124.
7. Herr, P.; Glaser, F.; Büldt, L. A.; Larsen, C. B.; Wenger, O. S., Long-Lived, Strongly Emissive, and Highly Reducing Excited States in Mo(0) Complexes with Chelating Isocyanides. *J. Am. Chem. Soc.* **2019,** *141*, 14394-14402.
8. Wenger, O. S., Photoactive Nickel Complexes in Cross-Coupling Catalysis. *Chem-Eur. J.* **2021,** *27*, 2270-2278.
9. Ting, S. I.; Garakyaraghi, S.; Taliaferro, C. M.; Shields, B. J.; Scholes, G. D.; Castellano, F. N.; Doyle, A. G., 3d-d Excited States of Ni(II) Complexes Relevant to Photoredox Catalysis: Spectroscopic Identification and Mechanistic Implications. *J. Am. Chem. Soc.* **2020,** *142*, 5800-5810.
10. Liu, T.; Tyburski, R.; Wang, S.; Fernández-Terán, R.; Ott, S.; Hammarström, L., Elucidating Proton-Coupled Electron Transfer Mechanisms of Metal Hydrides with Free Energy- and Pressure-Dependent Kinetics. *J. Am. Chem. Soc.* **2019,** *141*, 17245-17259.
11. Liu, T.; Guo, M.; Orthaber, A.; Lomoth, R.; Lundberg, M.; Ott, S.; Hammarström, L., Accelerating proton-coupled electron transfer of metal hydrides in catalyst model reactions. *Nature Chem.* **2018,** *10*, 881-887.
12. Zhang, Y.; Lee, T. S.; Favale, J. M.; Leary, D. C.; Petersen, J. L.; Scholes, G. D.; Castellano, F. N.; Milsmann, C., Delayed fluorescence from a zirconium(iv) photosensitizer with ligand-to-metal charge-transfer excited states. *Nature Chem.* **2020,** *12*, 345-352.
13. Zhang, Y.; Petersen, J. L.; Milsmann, C., A Luminescent Zirconium(IV) Complex as a Molecular Photosensitizer for Visible Light Photoredox Catalysis. *J. Am. Chem. Soc.* **2016,** *138*, 13115-13118.
14. Otto, S.; Grabolle, M.; Förster, C.; Kreitner, C.; Resch-Genger, U.; Heinze, K., [Cr(ddpd)2]3+: A Molecular, Water-Soluble, Highly NIR-Emissive Ruby Analogue. *Angew. Chem. Int. Ed.* **2015,** *54*, 11572-11576.
15. Otto, S.; Harris, J. P.; Heinze, K.; Reber, C., Molecular Ruby under Pressure. *Angew. Chem. Int. Ed.* **2018,** *57*, 11069-11073.
16. Büldt, L. A.; Guo, X.; Vogel, R.; Prescimone, A.; Wenger, O. S., A Tris(diisocyanide)chromium(0) Complex Is a Luminescent Analog of Fe(2,2′-Bipyridine)32+. *J. Am. Chem. Soc.* **2017,** *139*, 985-992.
17. Pal, A. K.; Li, C. F.; Hanan, G. S.; Zysman-Colman, E., Blue-Emissive Cobalt(III) Complexes and Their Use in the Photocatalytic Trifluoromethylation of Polycyclic Aromatic Hydrocarbons. *Angew. Chem. Int. Ed.* **2018,** *57,*, 8027−8031.
18. Kaufhold, S.; Rosemann, N. W.; Chábera, P.; Lindh, L.; Bolaño Losada, I.; Uhlig, J.; Pascher, T.; Strand, D.; Wärnmark, K.; Yartsev, A.; Persson, P., Microsecond Photoluminescence and Photoreactivity of a Metal-Centered Excited State in a Hexacarbene–Co(III) Complex. *J. Am. Chem. Soc.* **2021,** *143*, 1307-1312.
19. Woodhouse, M. D.; McCusker, J. K., Mechanistic Origin of Photoredox Catalysis Involving Iron(II) Polypyridyl Chromophores. *J. Am. Chem. Soc.* **2020,** *142*, 16229-16233.

20. Temperton, R. H.; Rosemann, N. W.; Guo, M.; Johansson, N.; Fredin, L. A.; Prakash, O.; Wärnmark, K.; Handrup, K.; Uhlig, J.; Schnadt, J.; Persson, P., Site-Selective Orbital Interactions in an Ultrathin Iron-Carbene Photosensitizer Film. *J. Phys. Chem. A* **2020,** *124*, 1603-1609.
21. Tatsuno, H.; Kjær, K. S.; Kunnus, K.; Harlang, T. C. B.; Timm, C.; Guo, M.; Chàbera, P.; Fredin, L. A.; Hartsock, R. W.; Reinhard, M. E.; Koroidov, S.; Li, L.; Cordones, A. A.; Gordivska, O.; Prakash, O.; Liu, Y.; Laursen, M. G.; Biasin, E.; Hansen, F. B.; Vester, P.; Christensen, M.; Haldrup, K.; Németh, Z.; Sárosiné Szemes, D.; Bajnóczi, É.; Vankó, G.; Van Driel, T. B.; Alonso-Mori, R.; Glownia, J. M.; Nelson, S.; Sikorski, M.; Lemke, H. T.; Sokaras, D.; Canton, S. E.; Dohn, A. O.; Møller, K. B.; Nielsen, M. M.; Gaffney, K. J.; Wärnmark, K.; Sundström, V.; Persson, P.; Uhlig, J., Hot Branching Dynamics in a Light-Harvesting Iron Carbene Complex Revealed by Ultrafast X-ray Emission Spectroscopy. *Angew. Chem. Int. Ed.* **2020,** *59*, 364-372.
22. Rosemann, N. W.; Chábera, P.; Prakash, O.; Kaufhold, S.; Wärnmark, K.; Yartsev, A.; Persson, P., Tracing the Full Bimolecular Photocycle of Iron(III)–Carbene Light Harvesters in Electron-Donating Solvents. *J. Am. Chem. Soc.* **2020,** *142*, 8565-8569.
23. Prakash, O.; Chábera, P.; Rosemann, N. W.; Huang, P.; Häggström, L.; Ericsson, T.; Strand, D.; Persson, P.; Bendix, J.; Lomoth, R.; Wärnmark, K., A Stable Homoleptic Organometallic Iron(IV) Complex. *Chem-Eur. J.* **2020,** *26*, 12728-12732.
24. Paulus, B. C.; Adelman, S. L.; Jamula, Lindsey L.; McCusker, James K., Leveraging excited-state coherence for synthetic control of ultrafast dynamics. *Nature* **2020,** *582*, 214-218.
25. McCusker, J. K., Electronic structure in the transition metal block and its implications for light harvesting. *Science* **2019,** *363*, 484-488.
26. Liu, Y.; Kjær, K. S.; Fredin, L. A.; Chábera, P.; Harlang, T.; Canton, S. E.; Lidin, S.; Zhang, J.; Lomoth, R.; Bergquist, K.-E.; Persson, P.; Wärnmark, K.; Sundström, V., A Heteroleptic Ferrous Complex with Mesoionic Bis(1,2,3-triazol-5-ylidene) Ligands: Taming the MLCT Excited State of Iron(II). *Chem-Eur. J.* **2015,** *21*, 3628-3639.
27. Liu, Y.; Harlang, T.; Canton, S. E.; Chábera, P.; Suárez-Alcántara, K.; Fleckhaus, A.; Vithanage, D. A.; Göransson, E.; Corani, A.; Lomoth, R.; Sundström, V.; Wärnmark, K., Towards longer-lived metal-to-ligand charge transfer states of iron(ii) complexes: an N-heterocyclic carbene approach. *Chem. Commun.* **2013,** *49*, 6412-6414.
28. Lindh, L.; Chábera, P.; Rosemann, N. W.; Uhlig, J.; Wärnmark, K.; Yartsev, A.; Sundström, V.; Persson, P., Photophysics and Photochemistry of Iron Carbene Complexes for Solar Energy Conversion and Photocatalysis. *Catalysts* **2020,** *10*, 315.
29. Kjær, K. S.; Kaul, N.; Prakash, O.; Chábera, P.; Rosemann, N. W.; Honarfar, A.; Gordivska, O.; Fredin, L. A.; Bergquist, K.-E.; Häggström, L.; Ericsson, T.; Lindh, L.; Yartsev, A.; Styring, S.; Huang, P.; Uhlig, J.; Bendix, J.; Strand, D.; Sundström, V.; Persson, P.; Lomoth, R.; Wärnmark, K., Luminescence and reactivity of a charge-transfer excited iron complex with nanosecond lifetime. *Science* **2019,** *363*, 249-253.
30. Jiang, Y.; Liu, L. C.; Sarracini, A.; Krawczyk, K. M.; Wentzell, J. S.; Lu, C.; Field, R. L.; Matar, S. F.; Gawelda, W.; Müller-Werkmeister, H. M.; Miller, R. J. D., Direct observation of nuclear reorganization driven by ultrafast spin transitions. *Nature Comm.* **2020,** *11*, 1530.
31. Jiang, T.; Bai, Y.; Zhang, P.; Han, Q.; Mitzi, D. B.; Therien, M. J., Electronic structure and photophysics of a supermolecular iron complex having a long MLCT-state lifetime and panchromatic absorption. *Proc. Natl. Acad. Sci. USA* **2020,** *117*, 20430-20437.
32. Harlang, T. C. B.; Liu, Y.; Gordivska, O.; Fredin, L. A.; Ponseca, C. S.; Huang, P.; Chábera, P.; Kjaer, K. S.; Mateos, H.; Uhlig, J.; Lomoth, R.; Wallenberg, R.; Styring, S.; Persson, P.; Sundström, V.; Wärnmark, K., Iron sensitizer converts light to electrons with 92% yield. *Nature Chem.* **2015,** *7*, 883-889.

33. Dierks, P.; Päpcke, A.; Bokareva, O. S.; Altenburger, B.; Reuter, T.; Heinze, K.; Kühn, O.; Lochbrunner, S.; Bauer, M., Ground- and Excited-State Properties of Iron(II) Complexes Linked to Organic Chromophores. *Inorg. Chem.* **2020,** *59*, 14746-14761.
34. Chábera, P.; Liu, Y.; Prakash, O.; Thyrhaug, E.; Nahhas, A. E.; Honarfar, A.; Essén, S.; Fredin, L. A.; Harlang, T. C. B.; Kjær, K. S.; Handrup, K.; Ericson, F.; Tatsuno, H.; Morgan, K.; Schnadt, J.; Häggström, L.; Ericsson, T.; Sobkowiak, A.; Lidin, S.; Huang, P.; Styring, S.; Uhlig, J.; Bendix, J.; Lomoth, R.; Sundström, V.; Persson, P.; Wärnmark, K., A low-spin Fe(iii) complex with 100-ps ligand-to-metal charge transfer photoluminescence. *Nature* **2017,** *543*, 695-699.
35. Braun, J. D.; Lozada, I. B.; Kolodziej, C.; Burda, C.; Newman, K. M. E.; van Lierop, J.; Davis, R. L.; Herbert, D. E., Iron(ii) coordination complexes with panchromatic absorption and nanosecond charge-transfer excited state lifetimes. *Nature Chem.* **2019,** *11*, 1144-1150.
36. Kaul, N.; Lomoth, R., The Carbene Cannibal: Photoinduced Symmetry-Breaking Charge Separation in an Fe(III) N-Heterocyclic Carbene. *J. Am. Chem. Soc.* **2021,** *143*, 10816-10821.
37. Kaufhold, S.; Wärnmark, K., Design and Synthesis of Photoactive Iron N-Heterocyclic Carbene Complexes. *Catalysts* **2020,** *10*, 132.
38. Chábera, P.; Kjaer, K. S.; Prakash, O.; Honarfar, A.; Liu, Y.; Fredin, L. A.; Harlang, T. C. B.; Lidin, S.; Uhlig, J.; Sundström, V.; Lomoth, R.; Persson, P.; Wärnmark, K., FeII Hexa N-Heterocyclic Carbene Complex with a 528 ps Metal-to-Ligand Charge-Transfer Excited-State Lifetime. *J. Phys. Chem. Lett.* **2018,** *9*, 459-463.
39. Xia, S.; Hu, K.; Lei, C.; Jin, J., Intramolecular Aromatic C–H Acyloxylation Enabled by Iron Photocatalysis. *Org. Lett.* **2020,** *22*, 1385-1389.
40. Li, S.; Zhu, B.; Lee, R.; Qiao, B.; Jiang, Z., Visible light-induced selective aerobic oxidative transposition of vinyl halides using a tetrahalogenoferrate(iii) complex catalyst. *Organic Chemistry Frontiers* **2018,** *5*, 380-385.
41. Huang, B.; Li, Y.; Yang, C.; Xia, W., Three-component aminoselenation of alkenes via visible-light enabled Fe-catalysis. *Green Chem.* **2020,** *22*, 2804-2809.
42. Gualandi, A.; Marchini, M.; Mengozzi, L.; Natali, M.; Lucarini, M.; Ceroni, P.; Cozzi, P. G., Organocatalytic Enantioselective Alkylation of Aldehydes with [Fe(bpy)3]Br2 Catalyst and Visible Light. *ACS Catal.* **2015,** *5*, 5927-5931.
43. Parisien-Collette, S.; Hernandez-Perez, A. C.; Collins, S. K., Photochemical Synthesis of Carbazoles Using an [Fe(phen)3](NTf2)2/O2 Catalyst System: Catalysis toward Sustainability. *Org. Lett.* **2016,** *18*, 4994-4997.
44. Narayanam, J. M. R.; Tucker, J. W.; Stephenson, C. R. J., Electron-Transfer Photoredox Catalysis: Development of a Tin-Free Reductive Dehalogenation Reaction. *J. Am. Chem. Soc.* **2009,** *131*, 8756-8757.
45. Michelet, B.; Deldaele, C.; Kajouj, S.; Moucheron, C.; Evano, G., A General Copper Catalyst for Photoredox Transformations of Organic Halides. *Org. Lett.* **2017,** *19*, 3576-3579.
46. Cerfontaine, S.; Wehlin, S. A. M.; Elias, B.; Troian-Gautier, L., Photostable Polynuclear Ruthenium(II) Photosensitizers Competent for Dehalogenation Photoredox Catalysis at 590 nm. *J. Am. Chem. Soc.* **2020,** *142*, 5549-5555.
47. Forshaw, A. P.; Bontchev, R. P.; Smith, J. M., Oxidation of the Tris(carbene)borate Complex PhB(MeIm)3MnI(CO)3 to MnIV[PhB(MeIm)3]2(OTf)2. *Inorg. Chem.* **2007,** *46*, 3792-3794.
48. We were unable to reproduce the reported 45% yield for the synthesis of 1+. The origin of this discrepancy is still unknown.
49. Nelsen, S. F.; Hintz, P. J., Electrochemical oxidation of tertiary amines. Effect of structure upon reversibility. *J. Am. Chem. Soc.* **1972,** *94*, 7114-7117.

50. Pellegrin, Y.; Odobel, F., Sacrificial electron donor reagents for solar fuel production. *Comptes Rendus Chimie* **2017,** *20*, 283-295.
51. Pischel, U.; Zhang, X.; Hellrung, B.; Haselbach, E.; Muller, P.-A.; Nau, W. M., Fluorescence Quenching of n,π*-Excited Azoalkanes by Amines: What Is a Sterically Hindered Amine? *J. Am. Chem. Soc.* **2000,** *122*, 2027-2034.
52. Luo, P.; Feinberg, E. C.; Guirado, G.; Farid, S.; Dinnocenzo, J. P., Accurate Oxidation Potentials of 40 Benzene and Biphenyl Derivatives with Heteroatom Substituents. *J. Org. Chem.* **2014,** *79*, 9297-9304.
53. Owano, H.; Murakami, H.; Yamashita, T.; Ohigashi, H.; Ogata, T., Electrodeposition of the cationic radical salts of some aromatic diamines from acetonitrile solution. *Synthetic Metals* **1991,** *39*, 327-341.
54. Troian-Gautier, L.; DiMarco, B. N.; Sampaio, R. N.; Marquard, S. L.; Meyer, G. J., Evidence that ΔS‡ Controls Interfacial Electron Transfer Dynamics from Anatase TiO2 to Molecular Acceptors. *J. Am. Chem. Soc.* **2018,** *140*, 3019-3029.
55. DiMarco, B. N.; Troian-Gautier, L.; Sampaio, R. N.; Meyer, G. J., Dye-sensitized electron transfer from TiO2 to oxidized triphenylamines that follows first-order kinetics. *Chem. Sci.* **2018,** *9*, 940-949.
56. Arias-Rotondo, D. M.; McCusker, J. K., The photophysics of photoredox catalysis: a roadmap for catalyst design. *Chem. Soc. Rev.* **2016,** *45*, 5803-5820.
57. Harriman, A.; Porter, G.; Wilowska, A., Photoreduction of benzo-1,4-quinone sensitised by metalloporphyrins. *J. Chem. Soc., Faraday Trans. 2* **1983,** *79*, 807-816.
58. Gould, I. R.; Moser, J. E.; Armitage, B.; Farid, S.; Goodman, J. L.; Herman, M. S., Electron-transfer reactions in the Marcus inverted region. Charge recombination versus charge shift reactions. *J. Am. Chem. Soc.* **1989,** *111*, 1917-1919.
59. Mandal, K.; Hoffman, M. Z., Solution medium control of the photoredox yield in the Ru(bpy)32+/methyl viologen/EDTA system. *J. Phys. Chem* **1984,** *88*, 185-187.
60. Olmsted, J.; Meyer, T. J., Factors affecting cage escape yields following electron-transfer quenching. *J. Phys. Chem* **1987,** *91*, 1649-1655.
61. Sutin, N.; Creutz, C., Light induced electron transfer reactions of metal complexes. *Pure and Applied Chemistry* **1980,** *52*, 2717-2738.
62. Hoffman, M. Z., Cage escape yields from the quenching of excited tris(bipyridyl)ruthenium(2+) by methylviologen in aqueous solution. *J. Phys. Chem* **1988,** *92*, 3458-3464.
63. S. Jayanthi, S.; Ramamurthy, P., Photoinduced electron transfer reactions of 2,4,6-triphenylpyrylium: solvent effect and charge-shift type of systems. *Phys. Chem. Chem. Phys.* **1999,** *1*, 4751-4757.
64. Manoj, N.; Ajit Kumar, R.; Gopidas, K. R., Photophysical and electron transfer studies of a few 2,6-dimethyl-4-(alkylphenyl)pyrylium and thiopyrylium derivatives. *J. Photoch. Photobio. A* **1997,** *109*, 109-118.
65. Wolff, H.-J.; Burssher, D.; Steiner, U. E., Spin-orbit coupling controlled spin chemistry of Ru(bpy)32+ photooxidation: Detection of strong viscosity dependence of in-cage backward electron transfer rate. *Pure and Applied Chemistry* **1995,** *67*, 167.
66. Lucia, L. A.; Schanze, K. S., Cage escape yields for photoinduced bimolecular electron transfer reactions of Re(I) complexes. *Inorg. Chim. Acta* **1994,** *225*, 41-49.
67. Juris, A.; Balzani, V.; Barigelletti, F.; Campagna, S.; Belser, P.; von Zelewsky, A., Ru(II) polypyridine complexes: photophysics, photochemistry, eletrochemistry, and chemiluminescence. *Coord. Chem. Rev.* **1988,** *84*, 85-277.
68. Thompson, D. W.; Ito, A.; Meyer, T. J., [Ru(bpy)3]2+* and other remarkable metal-to-ligand charge transfer (MLCT) excited states. *Pure and Applied Chemistry* **2013,** *85*, 1257-1305.

69. Troian-Gautier, L.; Mugeniwabagara, E.; Fusaro, L.; Moucheron, C.; Kirsch-De Mesmaeker, A.; Luhmer, M., pH Dependence of Photoinduced Electron Transfer with [Ru(TAP)3]2+. *Inorg. Chem.* **2017,** *56*, 1794-1803.
70. Troian-Gautier, L.; Mugeniwabagara, E.; Fusaro, L.; Cauët, E.; Kirsch-De Mesmaeker, A.; Luhmer, M., Photo-CIDNP Reveals Different Protonation Sites Depending on the Primary Step of the Photoinduced Electron-/Proton-Transfer Process with Ru(II) Polyazaaromatic Complexes. *J. Am. Chem. Soc.* **2017,** *139*, 14909-14912.
71. Cerfontaine, S.; Troian-Gautier, L.; Wehlin, S. A. M.; Loiseau, F.; Cauët, E.; Elias, B., Tuning the excited-state deactivation pathways of dinuclear ruthenium(ii) 2,2′-bipyridine complexes through bridging ligand design. *Dalton Trans.* **2020,** *49*, 8096-8106.
72. Cerfontaine, S.; Troian-Gautier, L.; Duez, Q.; Cornil, J.; Gerbaux, P.; Elias, B., MLCT Excited-State Behavior of Trinuclear Ruthenium(II) 2,2′-Bipyridine Complexes. *Inorg. Chem.* **2021,** *60*, 366-379.
73. Bevernaegie, R.; Wehlin, S. A. M.; Elias, B.; Troian-Gautier, L., A Roadmap Towards Visible Light Mediated Electron Transfer Chemistry with Iridium(III) Complexes. *ChemPhotoChem* **2021,** *5*, 217-234.
74. Kalyanasundaram, K.; Neumann-Spallart, M., Influence of added salts on the cage escape yields in the photoredox quenching of Ru(bpy)2+3 excited states. *Chem. Phys. Lett.* **1982,** *88*, 7-12.
75. Adams, R. E.; Schmehl, R. H., Micellar Effects on Photoinduced Electron Transfer in Aqueous Solutions Revisited: Dramatic Enhancement of Cage Escape Yields in Surfactant Ru(II) Diimine Complex/[Ru(NH3)6]2+ Systems. *Langmuir* **2016,** *32*, 8598-8607.
76. van Willigen, H.; Jones, G.; Farahat, M. S., Time-Resolved EPR Study of Photoexcited Triplet-State Formation in Electron-Donor-Substituted Acridinium Ions. *J. Phys. Chem* **1996,** *100*, 3312-3316.
77. Martinho, J. M. G., Heavy-atom quenching of monomer and excimer pyrene fluorescence. *J. Phys. Chem* **1989,** *93*, 6687-6692.
78. Benniston, A. C.; Harriman, A.; Rostron, J. P., The effect of solvent polarity on the photophysical properties of 4-cyano-(4′-methylthio)diphenylacetylene: A prototypic donor–acceptor system. *Phys. Chem. Chem. Phys.* **2005,** *7*, 3041-3047.
79. Benniston, A. C.; Harriman, A.; Li, P.; Rostron, J. P.; van Ramesdonk, H. J.; Groeneveld, M. M.; Zhang, H.; Verhoeven, J. W., Charge Shift and Triplet State Formation in the 9-Mesityl-10-methylacridinium Cation. *J. Am. Chem. Soc.* **2005,** *127*, 16054-16064.
80. Wehlin, S. A. M.; Troian-Gautier, L.; Sampaio, R. N.; Marcélis, L.; Meyer, G. J., Ter-Ionic Complex that Forms a Bond Upon Visible Light Absorption. *J. Am. Chem. Soc.* **2018,** *140*, 7799-7802.
81. Troian-Gautier, L.; Beauvilliers, E. E.; Swords, W. B.; Meyer, G. J., Redox Active Ion-Paired Excited States Undergo Dynamic Electron Transfer. *J. Am. Chem. Soc.* **2016,** *138*, 16815-16826.
82. Scott, A. M.; Pyati, R., Solvent Viscosity and Interrelated Effects on Electrochemiluminescence Intensity of Tris(2,2‘-bipyridyl)ruthenium(II). *J. Phys. Chem. B* **2001,** *105*, 9011-9015.
83. Reynolds, E. W.; Demas, J. N.; DeGraff, B. A., Viscosity and Temperature Effects on the Rate of Oxygen Quenching of Tris-(2,2′-bipyridine)ruthenium(II). *J. Fluoresc.* **2013,** *23*, 237-241.
84. Neufeld, A. A.; Burshtein, A. I.; Angulo, G.; Grampp, G., Viscosity dependence of geminate recombination efficiency after bimolecular charge separation. *J. Chem. Phys.* **2002,** *116*, 2472-2479.
85. Burshtein, A. I.; Shokhirev, N. V., Viscosity and Free Energy Dependence of Photochemical Charge Separation. *J. Phys. Chem. A* **1997,** *101*, 25-30.

86. Shan, B.; Schmehl, R., Photochemical Generation of Strong One-Electron Reductants via Light-Induced Electron Transfer with Reversible Donors Followed by Cross Reaction with Sacrificial Donors. *J. Phys. Chem. A* **2014,** *118*, 10400-10406.
87. DeLaive, P. J.; Foreman, T. K.; Giannotti, C.; Whitten, D. G., Photoinduced electron transfer reactions of transition-metal complexes with amines. Mechanistic studies of alternate pathways to back electron transfer. *J. Am. Chem. Soc.* **1980,** *102*, 5627-5631.
88. Sampaio, R. N.; Grills, D. C.; Polyansky, D. E.; Szalda, D. J.; Fujita, E., Unexpected Roles of Triethanolamine in the Photochemical Reduction of CO2 to Formate by Ruthenium Complexes. *J. Am. Chem. Soc.* **2020,** *142*, 2413-2428.
89. Rees, N. V.; Klymenko, O. V.; Compton, R. G.; Oyama, M., The electro-oxidation of N,N-dimethyl-p-toluidine in acetonitrile:: a microdisk voltammetry study. *J. Electroanal. Chem.* **2002,** *531*, 33-42.
90. Cao, F.; Kim, J.; Bard, A. J., Detection of the Short-Lived Cation Radical Intermediate in the Electrochemical Oxidation of N,N-Dimethylaniline by Scanning Electrochemical Microscopy. *J. Am. Chem. Soc.* **2014,** *136*, 18163-18169.
91. Wang, P.-Z.; Chen, J.-R.; Xiao, W.-J., Hantzsch esters: an emerging versatile class of reagents in photoredox catalyzed organic synthesis. *Org. Biomol. Chem.* **2019,** *17*, 6936-6951.
92. Konev, M. O.; Cardinale, L.; Jacobi von Wangelin, A., Catalyst-Free N-Deoxygenation by Photoexcitation of Hantzsch Ester. *Org. Lett.* **2020,** *22*, 1316-1320.
93. Chen, W.; Tao, H.; Huang, W.; Wang, G.; Li, S.; Cheng, X.; Li, G., Hantzsch Ester as a Photosensitizer for the Visible-Light-Induced Debromination of Vicinal Dibromo Compounds. *Chem-Eur. J.* **2016,** *22*, 9546-9550.
94. Gu, F.; Huang, W.; Liu, X.; Chen, W.; Cheng, X., Substituted Hantzsch Esters as Versatile Radical Reservoirs in Photoredox Reactions. *Advanced Synthesis & Catalysis* **2018,** *360*, 925-931.
95. Heredia, M. D.; Guerra, W. D.; Barolo, S. M.; Fornasier, S. J.; Rossi, R. A.; Budén, M. E., Transition-Metal-Free and Visible-Light-Mediated Desulfonylation and Dehalogenation Reactions: Hantzsch Ester Anion as Electron and Hydrogen Atom Donor. *J. Org. Chem.* **2020,** *85*, 13481-13494.
96. Li, Z.; Yang, J.-D.; Cheng, J.-P., Thermodynamic and kinetic studies of hydride transfer from Hantzsch ester under the promotion of organic bases. *Organic Chemistry Frontiers* **2021,** *8*, 876-882.
97. Park, G.; Yi, S. Y.; Jung, J.; Cho, E. J.; You, Y., Mechanism and Applications of the Photoredox Catalytic Coupling of Benzyl Bromides. *Chem-Eur. J.* **2016,** *22*, 17790-17799.

For Table of Contents Only

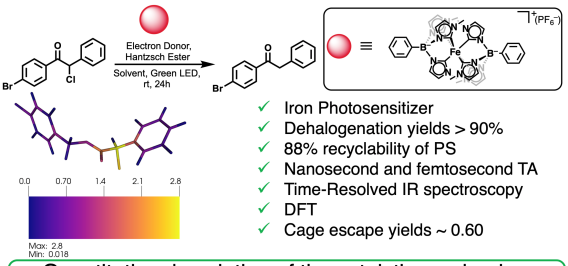

- ✓ Iron Photosensitizer
- ✓ Dehalogenation yields > 90%
- ✓ 88% recyclability of PS
- ✓ Nanosecond and femtosecond TA
- ✓ Time-Resolved IR spectroscopy
- ✓ DFT
- ✓ Cage escape yields ~ 0.60

Quantitative description of the catalytic mechanism with associated rate constants and yields